

Non-Hermitian sensing in the absence of exceptional points

Lei Xiao,^{1,2,*} Yaoming Chu,^{3,*} Quan Lin,² Haiqing Lin,⁴ Wei Yi,^{5,6,†} Jianming Cai,^{3,‡} and Peng Xue^{1,2,§}

¹*School of Physics, Southeast University, Nanjing 211189, China*

²*Beijing Computational Science Research Center, Beijing 100193, China*

³*School of Physics, International Joint Laboratory on Quantum Sensing and Quantum Metrology, Hubei Key Laboratory of Gravitation and Quantum Physics,*

Institute for Quantum Science and Engineering, Wuhan National High Magnetic Field Center,

Huazhong University of Science and Technology, Wuhan 430074, China

⁴*School of Physics, Zhejiang University, Hangzhou 310030, China*

⁵*CAS Key Laboratory of Quantum Information, University of Science and Technology of China, Hefei 230026, China*

⁶*CAS Center For Excellence in Quantum Information and Quantum Physics, Hefei 230026, China*

Open systems possess unique potentials in high-precision sensing, yet the majority of previous studies rely on the spectral singularities known as exceptional points. Here we theoretically propose and experimentally demonstrate universal non-Hermitian sensing in the absence of exceptional points. The scheme makes use of the intrinsic sensitivity of a non-Hermitian probe to weak external fields, which can be understood as the direct consequence of non-Hermiticity. We confirm the basic mechanism by simulating the sensor-field dynamics using photon interferometry, and, as a concrete example, demonstrate the enhanced sensing of signals encoded in the setting angle of a wave plate. While the sensitivity of the probe is ultimately limited by the measurement noise, we find the non-Hermitian sensor showing superior performance under background noises that cannot be suppressed through repetitive measurements. Our experiment opens the avenue of enhanced sensing without exceptional points, complementing existing efforts aimed at harnessing the unique features of open systems.

Introduction.—High-precision sensing plays an increasingly important role in modern science, and much effort has been invested in designing novel sensing schemes and next-generation sensors [1, 2]. A promising route is to exploit the unique sensitivity of open systems to external perturbations, of which an outstanding example is exceptional-point (EP)-based sensing [3–24]. While the dynamics of open systems can be described by non-Hermitian effective Hamiltonians, their complex eigenspectra exhibit exotic degeneracies at the branch-point singularities known as the EPs [25–27]. A system can exhibit fascinating properties near an EP, where, importantly, the eigenspectra become highly susceptible to weak perturbations, a feature that has been extensively researched for EP-enhanced sensing. Over the past decades, proof-of-principle EP-enhanced sensors have been demonstrated using classical electromagnetic or acoustic waves [28–38], and in quantum open systems of trapped ions [39], solid spins [40], or single photons [41]. These prototype sensors and their underlying protocols vitally depend on the presence of EPs, necessitating specific designs of non-Hermitian effective Hamiltonians with fine-tuned parameters.

In this work, we propose and demonstrate non-Hermitian sensing in the absence of EPs. The scheme relies on the non-Hermiticity-enhanced susceptibility of physical observables to weak perturbations, which, distinct from the EP-based sensitivity, is a generic feature of non-Hermitian systems, making the sensing scheme universal [42]. Using a cyclic photonic interferometer, we experimentally simulate the discrete-time dynamics of the probe-field system with tunable non-Hermiticity.

We observe enhanced sensitivity under a non-Hermitian setting, thus confirming the feasibility of our scheme. To provide a prototype scenario for application, we then demonstrate the sensing of signals encoded in the setting angle of a wave plate. We also theoretically analyze and experimentally confirm the superiority of the non-Hermitian sensing scheme—it outperforms its Hermitian counterpart in the presence of background noises that do not average out through repetitive measurements.

Theoretical framework.—We consider a generic non-Hermitian qubit sensor perturbed by a weak external field, with the overall Hamiltonian given by $H = \mathcal{H} + \lambda V$, and λ denotes the small parameter to be estimated. In a properly chosen orthonormal basis denoted by $\{|0\rangle, |1\rangle\}$, the Hamiltonian of the bare non-Hermitian sensor can be generally expressed as (up to an arbitrary constant)

$$\mathcal{H} = \frac{2\mathcal{E}}{1+a} \begin{pmatrix} 1 & a \\ \delta & a \end{pmatrix} \quad (1)$$

with $|a| \leq 1$. Its two eigenstates are given by $|\phi_+\rangle \sim |0\rangle + \delta|1\rangle$ and $|\phi_-\rangle \sim |0\rangle - (\delta/a)|1\rangle$, respectively, with an associated energy splitting $2\mathcal{E}$. Importantly, our sensing scheme assumes the condition $|\delta| \ll 1$, which is always possible by a proper choice of the basis. Since the requirement of $\mathcal{E} \rightarrow 0$ is released, the non-Hermitian sensor under study is independent of the properties of any EPs.

We first focus on the unperturbed system dynamics governed by \mathcal{H} with the sensor initialized in the basis state, $|\psi(0)\rangle = |0\rangle$. The time-evolved state can then be written as

$$|\psi(t)\rangle = e^{-i\mathcal{H}t}|\psi(0)\rangle = \frac{1 - e^{i2\mathcal{E}t}}{1+a} (\mathcal{D}_t|0\rangle + \delta|1\rangle), \quad (2)$$

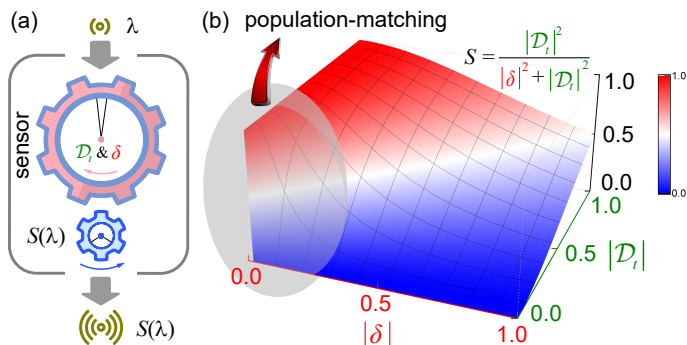


FIG. 1. Mechanism of the non-Hermiticity-enhanced sensing. (a) Schematic of the workflow. Within the sensor's range, a tiny variation in an external parameter λ leads to small changes in the sensor, parameterized by \mathcal{D}_t and δ . These changes further give rise to significant variations in a detectable $S(\lambda)$. (b) A qubit sensor is initialized in the basis state $|0\rangle$, close to an eigenstate (denoted as $|\phi_+\rangle$) of its non-Hermitian Hamiltonian, with $|\phi_+\rangle \sim |0\rangle + \delta|1\rangle$ and $|\delta| \ll 1$ is a parameter of the non-Hermitian sensor. Under a weak perturbation, the sensor generically evolves into the state $|\psi(t)\rangle \sim \mathcal{D}_t|0\rangle + \delta|1\rangle$. Generally, when the parameter \mathcal{D}_t is in the same order as δ , with $|\mathcal{D}_t| \sim |\delta| \ll 1$, the final population in state $|0\rangle$ (denoted as S) exhibits a sensitive reliance on the small parameters $|\delta|$ or \mathcal{D}_t , thus offering a practical probe for these parameters.

where $2\mathcal{D}_t = (1 - a) + i(1 + a) \cot \mathcal{E}t$. The population in the state $|0\rangle$ is straightforwardly determined by

$$S = \frac{|\mathcal{D}_t|^2}{|\delta|^2 + |\mathcal{D}_t|^2}. \quad (3)$$

Now, consider the time evolution under H , where an additional weak field is present. The parameters of the time-evolved state $\{\delta, a, \mathcal{E}\}$ all become λ -dependent, so is the normalized population in $|0\rangle$, which we denote as $S(\lambda)$. Its sensitivity to λ is captured by the susceptibility $\chi_\lambda = \partial_\lambda S(\lambda)$, which can be decomposed into

$$\chi_\lambda = \chi_{|\delta|} \partial_\lambda |\delta| + \chi_{|\mathcal{D}_t|} \partial_\lambda |\mathcal{D}_t|, \quad (4)$$

where $\chi_{|\delta|}$ and $\chi_{|\mathcal{D}_t|}$ are responses of S to variations in the parameters $|\delta|$ and \mathcal{D}_t , respectively.

As illustrated by Fig. 1, in the region $|\mathcal{D}_t| \sim |\delta| \ll 1$, $S(\lambda)$ shows fast variations with respect to $|\delta|$ and $|\mathcal{D}_t|$, thus also features a highly sensitive response to λ . Specifically, in the region with $|\mathcal{D}_t| \simeq |\delta| \ll 1$, the populations in the states $|0\rangle$ and $|1\rangle$ are comparable to each other. Due to the smallness of δ and \mathcal{D}_t , a weak perturbation (characterized by λ) could take the non-Hermitian sensor out of this region, causing a significant change in the signal.

The above population-matching condition (namely $|\mathcal{D}_t| \sim |\delta| \ll 1$) is achieved by exploiting the generic non-Hermiticity of the sensor, inherently facilitated by the non-orthogonal eigenstates and complex eigenvalues. For example, the non-orthogonality of eigenstates in a

pseudo-Hermitian system (where \mathcal{E} is real) allows a to be of the order unity ($a \approx 1$), which straightforwardly yields $\mathcal{D}_t \approx i \cot \mathcal{E}t$ [42]. When the evolution time is close to $\mathcal{E}t \simeq \frac{\pi}{2}$, $|\mathcal{D}_t|$ could be on the order of $|\delta|$, satisfying the population-matching condition. More general non-Hermitian sensing configurations beyond the pseudo-Hermitian case can also be established based on the population-matching condition [43].

The observations above form the basis of our non-Hermiticity-enhanced sensing scheme, which is fundamentally different from the previously reported EP-enhanced sensing [3, 4]. While the latter typically relies on the sensitivity of eigenstates and eigenvalues close to the EP, our scheme exploits the non-Hermitian sensing region illustrated in Fig. 1, which is emergent from the non-Hermitian dynamics starting from a specific initial state in the close proximity to an eigenstate of the unperturbed system.

However, the above discussion does not hold for a Hermitian system, where a unitary time evolution gives $2\mathcal{D}_t \approx 1 + i \cot \mathcal{E}t$ (where $a = \delta^2 \ll 1$), and thus $2|\mathcal{D}_t| \geq 1$. More specifically, we consider an exemplary Hermitian sensor, where the full Hamiltonian is given by $H_s = \lambda \sigma_x$. The time-evolved state follows the form of Eq. (2), by taking $\delta = 1$ and $\mathcal{D}_t = -i \cot \lambda t$, corresponding to the smooth non-sensitive region in Fig. 1. The normalized population in state $|0\rangle$ is

$$S(\lambda) = \frac{1}{2} (1 + \cos 2\lambda t). \quad (5)$$

The advantage of the non-Hermitian sensor is clearly revealed by comparing the susceptibilities defined in Eqs. (4) and (5), respectively, the latter being a smooth-varying sinusoidal.

Experiment implementation.—As a paradigmatic example, we experimentally implement the pseudo-Hermitian sensor described above using linear optics, dividing the process into many segments, each of which simulates a fixed time evolution governed by a pseudo-Hermitian Hamiltonian. The process can be extended to a real-time evolution and is regarded as a genuine quantum simulation in linear optics [44].

In our experiment, we encode the qubit basis in the horizontal and vertical polarization states of photons, i.e., $|0\rangle \equiv |H\rangle$ and $|1\rangle \equiv |V\rangle$. As illustrated in Fig. 2, our experimental setup includes three stages: state initialization, time evolution, and projective measurement. The wave packets of photons are generated by a pulsed laser source with a central wavelength of 808nm, a pulse width of 88ps, and a repetition rate of 31.25kHz. The pulses are attenuated to the single-photon level using neutral density filters. The photons are projected into the initial state $|H\rangle$ via a polarizing beam splitter (PBS) and then coupled in and out of an interferometric network through a low-reflectivity beam splitter (BS, reflectivity 10%), for time evolutions under the non-Hermitian Hamiltonian.

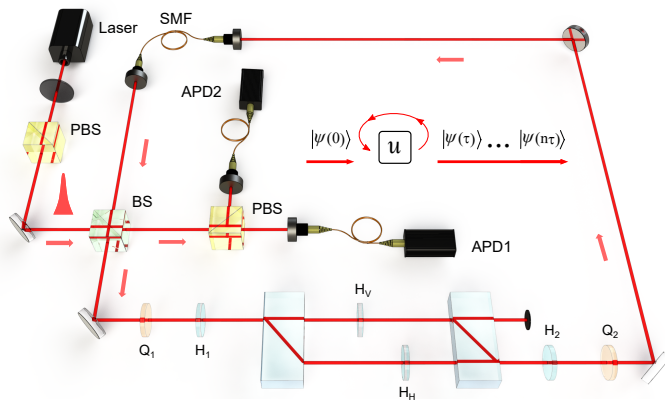


FIG. 2. Experimental schematic of the non-Hermitian cyclic-structure quantum evolution. A pulse laser is attenuated to the single-photon level via a set of neutral density filters and coupled into the cyclic quantum simulator through a beam splitter (BS). The non-unitary evolution operator u is implemented by a series of optical elements. After each evolution u , about 10% photons are reflected by the BS for projective measurement and the transmitted photons continue to go through the next cycle. The cyclic evolution process is depicted in the inset diagram. The state of the sensor is described as $|\psi(n\tau)\rangle = u(n\tau)|\psi(0)\rangle$.

Each segment of the time evolution is realized by the interferometric network involving several wave plates and two beam displacers (BDs). Such an interferometric network is capable of realizing an arbitrary 2×2 non-unitary operator [45–47].

We implement a stroboscopic simulation of the non-Hermitian dynamics, partitioning the overall evolution time t into n short segments $t = n\tau$. In our experiment, we choose $a = 1$ and $n = 5$. The non-unitary time evolution operator in each segment is

$$u(\tau) = e^{-i(H - \mathcal{E}\mathbb{I})\tau} = \begin{pmatrix} \cos \alpha\tau & -i\frac{\beta}{\alpha\delta} \sin \alpha\tau \\ -i\frac{\beta}{\alpha} \sin \alpha\tau & \cos \alpha\tau \end{pmatrix}, \quad (6)$$

where $\alpha = \sqrt{(\mathcal{E}\delta + \lambda)(\mathcal{E} + \delta\lambda)}/\delta$ and $\beta = \mathcal{E}\delta + \lambda$. For the implementation of u , we further decompose it according to

$$u = R_2(\theta_2, \phi_2) L(\theta_H, \theta_V) R_1(\theta_1, \phi_1), \quad (7)$$

where the rotation operator $R_i(\theta_i, \phi_i)$ ($i = 1, 2$) is realized by a quarter-wave plate (QWP) at ϕ_i and a half-wave plate (HWP) at θ_i , and the polarization-dependent loss operator L is realized by a combination of two BDs and a pair of HWPs at θ_H and θ_V . By adjusting the parameters of wave plates, we can simulate dynamics under Hamiltonians with tunable non-Hermiticity.

Each segment of the time evolution $u(\tau)$ is repeated through an optical cycle, in which photons propagate both in free space and through single-mode fibers. At the end of each cycle, the photons are re-coupled into the interferometric network through a low-reflectivity BS. The

transmitted photons recycle for the next segment, while about 10% of the photons are reflected and coupled out of the cycle and into the measurement module.

Finally, after photons have completed multiple cycles and are coupled out of the network by the BS, they register clicks at an avalanche photo-diode (APD) with a time jitter of 350ps for detection. The population of photons is obtained through projective measurement, which consists of a PBS and APDs. The counts of the horizontally polarized photons N_H and vertically polarized ones N_V are registered in the measurement stage and are used to determine susceptibilities in our experiment.

Measuring susceptibility.—We construct the normalized population of state $|H\rangle$ through the measured photon counts N_H and N_V , with

$$\bar{S} = \frac{N_H}{N_H + N_V}. \quad (8)$$

The populations of the state $|H\rangle$ after 5 segments of the time evolution governed by non-Hermitian and Hermitian Hamiltonians with the initial state $|H\rangle$ are shown in Figs. 3(a) and 3(c), respectively. In the non-Hermitian case, the population changes more sharply compared to its Hermitian counterpart, with respect to small variations in λ , especially when $\lambda/\varepsilon \in [-1.402, 1.832]$.

In Figs. 3(b) and 3(d), we show the measured susceptibility χ_λ as a function of λ/ε for both the non-Hermitian and Hermitian sensors. Since we take discretized values of λ in our experiment, the susceptibility is numerically estimated according to

$$\chi_{\lambda_i} = \frac{\bar{S}(\lambda_{i+1}) - \bar{S}(\lambda_i)}{\lambda_{i+1} - \lambda_i}, \quad (9)$$

where the subscript i represents the data index. As illustrated in Fig. 3(b), for the non-Hermitian sensor, we have the measured susceptibility $|\chi_\lambda| \leq 1018 \pm 97$. Whereas for the Hermitian case in Fig. 3(d), the measured susceptibility $|\chi_\lambda| \leq 262 \pm 9$. Therefore, the non-Hermitian sensor demonstrates a remarkable advantage for the estimation of λ .

An application.—In the experiment above, the external field V is simulated by a set of linear optical elements, and the adjustment of the parameter λ is realized by tuning the setting angles of the combination of wave plates (H_1 , H_2 and H_V). As a primordial demonstration of non-Hermitian sensing, we now encode the signal λ in the setting angle of a single wave plate. Our goal is to estimate the parameter θ_1 of the wave plate H_1 with the non-Hermitian sensor. For this purpose, photons are initialized in the state $|\psi(0)\rangle = |H\rangle$. We fix the setting angles of the other wave plates as $\varphi_1 = 0.5\pi$, $\varphi_2 = -0.5\pi$, $\theta_2 = 0.03\pi$, $\theta_V = 0.43\pi$, which are determined by numerical simulations and optimization analysis. The populations of the state $|H\rangle$ after 5 segments of the time evolution governed by the non-Hermitian Hamiltonian with

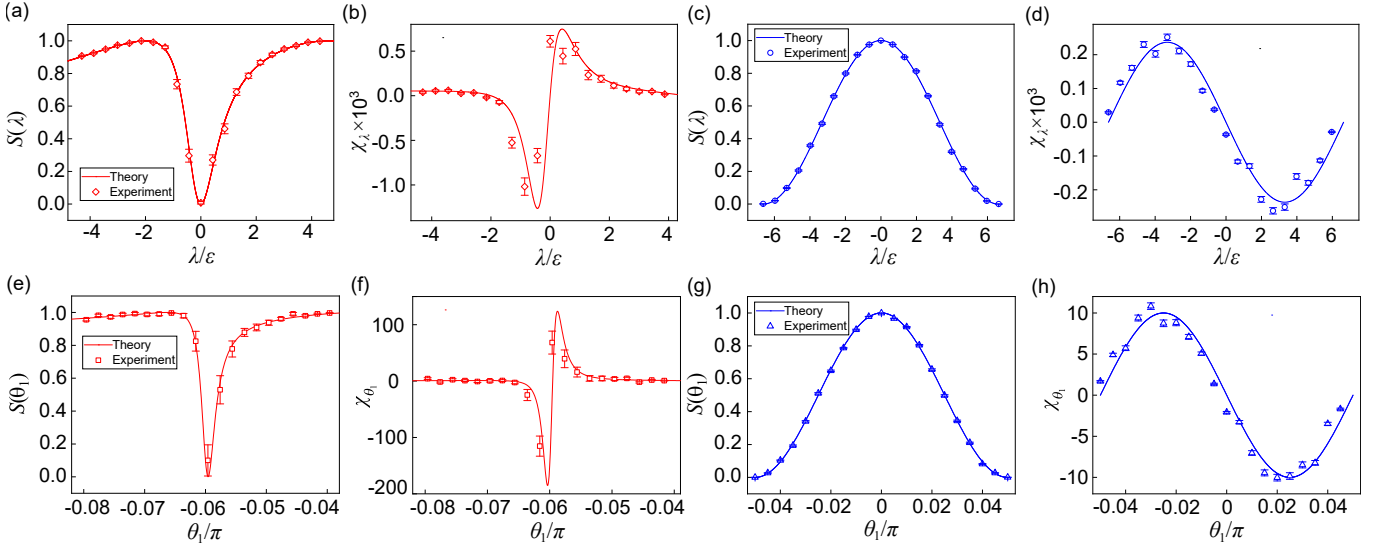


FIG. 3. Experimental results of the susceptibility of non-Hermitian and Hermitian sensors. The normalized population $S(\lambda)$ of the state $|H\rangle$ and the susceptibility χ_λ as a function of λ for the non-Hermitian sensor (a)-(b) and its Hermitian counterpart (c)-(d), respectively. The normalized population $S(\theta_1)$ and the susceptibility χ_{θ_1} as a function of θ_1 for the non-Hermitian sensor (e)-(f) and its Hermitian counterpart (g)-(h), respectively. Symbols represent the experimental data and lines are the corresponding theoretical predictions with the initial state $|H\rangle$ and the evolution time $t = \pi/2\mathcal{E}$. Other parameters are $\delta = 0.3015$, $\mathcal{E} = \delta/50$ and $\varepsilon = 0.001$. Error bars are due to the statistical uncertainty in photon number counting.

the initial state $|H\rangle$ are shown in Fig. 3(e). Apparently, the measured population becomes more sensitive to θ_1 around $\theta_1 = -0.06\pi$. The susceptibility χ_{θ_1} is calculated from the measured population and shown in Fig. 3(f). The maximum value of the susceptibility is 115 ± 18 .

For comparison, we use a Hermitian sensor for the same task. We remove the BDs along with H_2 , H_H , and H_V , leaving wave plates $Q_2(\phi_2)$ - $H_1(\theta_1)$ - $Q_1(\phi_1)$. We fix the setting angles of the wave plates to be the same as those of the non-Hermitian sensor, with $\varphi_1 = 0.5\pi$, $\varphi_2 = -0.5\pi$. Figures 3(g) and 3(h) show the population and the susceptibility of the Hermitian sensor. The measured susceptibility is $|\chi_{\theta_1}| \leq 10.8 \pm 0.4$. Hence, the non-Hermitian enhancement ratio is ~ 10.6 .

Non-Hermitian sensing under noise.—Noise is a fundamental challenge for sensors as the sensitivity of a sensor is ultimately limited by noise. Generally, the influence of measurement noises on the sensitivity of the non-Hermitian sensor can be eliminated by repeating the measurement. However, for systematic noises that cannot be averaged out, the non-Hermitian sensors demonstrated here also outperform the Hermitian ones. In the following, we take background noises [48, 49] as an example, and experimentally confirm the non-Hermitian advantage.

We characterize the measurement sensitivity ΔS using the standard deviation of the parameter to be estimated. The measurement sensitivity indicates the minimum change of the parameter that can be distinguished in the presence of the background noise. This allows us to directly compare the non-Hermitian sensing protocols

to more established methods. For simplicity, we focus on the background noise due to the imperfection of detectors. The measured population of the state $|H\rangle$ in Eq. (8) is then modified as

$$\begin{aligned} \bar{S}' &= \frac{N_H + N'_H}{N_H + N'_H + N_V + N'_V} \\ &\approx \bar{S} + (1 - \bar{S}) \frac{N'_H}{N} - \bar{S} \frac{N'_V}{N}. \end{aligned} \quad (10)$$

Here $N'_{H,V}$ represents the additional photon numbers in the corresponding polarization states caused by the background noise, and $N = N_H + N_V$. In general, the background noise is completely random. The corresponding photon numbers are therefore given by $N'_H \in [0, \eta_H N]$ and $N'_V \in [0, \eta_V N]$, respectively. Applying error propagation on Eq. (10), the standard deviation of \bar{S}' is

$$\begin{aligned} \Delta \bar{S}'^2 &= \left(\frac{\partial \bar{S}'}{\partial \bar{S}} \Delta \bar{S} \right)^2 + \left(\frac{\partial \bar{S}'}{\partial N'_H/N} \Delta \frac{N'_H}{N} \right)^2 + \left(\frac{\partial \bar{S}'}{\partial N'_V/N} \Delta \frac{N'_V}{N} \right)^2 \\ &= \left(1 - \frac{\eta_H + \eta_V}{2} \right)^2 \Delta \bar{S}^2 + \frac{1}{12} [(1 - \bar{S})^2 \eta_H^2 + \bar{S}^2 \eta_V^2]. \end{aligned} \quad (11)$$

The first term on the right-hand side of Eq. (S6) (in the second line) comes from the fluctuation of photons, which can be averaged out through repetitive measurements. Namely, the term tends to zero when $N \gg 1$. By contrast, the second term comes from the background noise, which is independent of N and cannot be averaged out.

We experimentally demonstrate the performance of the non-Hermitian sensor in the presence of background

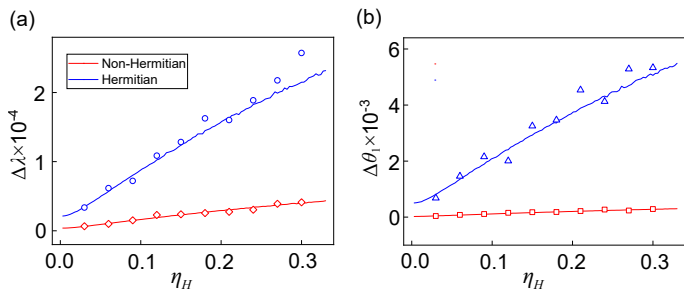


FIG. 4. Experimental results of the measurement uncertainty. Measured standard deviation $\Delta\lambda$ in (a) and $\Delta\theta_1$ in (b) as a function of the strength η_H of the background noise. Symbols representing the results are obtained by repeating measurements for 50 times for each of the noise strengths chosen in our experiment. The lines are numerical simulations that are obtained from 10000 measurements for each noise strength.

noise. We use two light-emitting diode (LED) which are placed close to the APDs, to simulate the background noise. We adjust the intensity of the LEDs to ensure that the changes in $N'_{H,V}$ are proportional to N . For simplicity, we choose $\eta_V = 1.2\eta_H$. We choose the working point of the sensor, i.e., λ corresponding to $|\chi_\lambda|_{\max}$, and repeat measurements for 50 times for each of the noise strengths chosen in our experiment. For the measured population of the state $|H\rangle$, we calculate the standard deviation $\Delta\bar{S}'$ based on Eq. (S6) and $\Delta\lambda = \Delta\bar{S}'/|\chi_\lambda|_{\max}$ through the propagation of error.

In Fig. 4, we show how the measurement uncertainty varies as a function of the noise strength η_H , for both the non-Hermitian and Hermitian sensors. The results show that, with increasing noise strength, the measurement sensitivity $\Delta\lambda$ ($\Delta\theta_1$) deteriorates in both cases. However, $\Delta\lambda$ ($\Delta\theta_1$) of the non-Hermitian sensor is always smaller compared to the Hermitian one. Thus, the non-Hermitian sensor possesses enhanced sensitivity compared to the Hermitian counterpart in the presence of background noise. As such, non-Hermiticity allows one to enhance the measurement sensitivity, over a conventional Hermitian sensor, both with and without noise.

Conclusion.—We propose and demonstrate a generic non-Hermitian sensing scheme that does not rely on the presence of EPs. Simulating the non-Hermitian dynamics of the sensor-field system, we show that the non-Hermitian sensor is superior to its Hermitian counterpart, both in terms of susceptibility, and in terms of performance against background noise. While the non-Hermitian sensor in our experiment is time-independent, it is possible to achieve time dependence through electro-optical modulators, which should open up fresh opportunities for novel sensor design. Furthermore, while our demonstration is performed on the single-qubit level, it is possible to extend the sensing scheme to multi-qubit cases. Our work thus paves the way toward a new class of non-Hermitian sensors.

This work is supported by the National Key R&D Program of China (Grant No. 2023YFA1406701), National Natural Science Foundation of China (Grants No. 92265209, No. 12025401, No. 12304572, and No. 12104036) and the fellowship of China Postdoctoral Science Foundation (Grant No. 2022M721256).

* These authors contributed equally to this work.

† wyiz@ustc.edu.cn

‡ jianmingcai@hust.edu.cn

§ gnep.eux@gmail.com

- [1] A. C. Tam, Applications of photoacoustic sensing techniques, *Rev. Mod. Phys.* **58**, 381-431 (1986).
- [2] C. L. Degen, F. Reinhard and P. Cappellaro, Quantum sensing, *Rev. Mod. Phys.* **89**, 035002 (2017).
- [3] J. Wiersig, Enhancing the sensitivity of frequency and energy splitting detection by using exceptional points: Application to microcavity sensors for single-particle detection, *Phys. Rev. Lett.* **112**, 203901 (2014).
- [4] J. Wiersig, Sensors operating at exceptional points: General theory, *Phys. Rev. A* **93**, 033809 (2016).
- [5] Z. P. Liu, J. Zhang, Ş. K. Özdemir, B. Peng, H. Jing, X. Y. Lü, C. W. Li, L. Yang, F. Nori and Y. X. Liu, Metrology with \mathcal{PT} -symmetric cavities: Enhanced sensitivity near the \mathcal{PT} -phase transition, *Phys. Rev. Lett.* **117**, 110802 (2016).
- [6] J. Ren, H. Hodaie, G. Harari, A. U. Hassan, W. Chow, M. Soltani, D. Christodoulides and M. Khajavikhan, Ultrasensitive micro-scale parity-time-symmetric ring laser gyroscope, *Opt. Lett.* **42**, 1556-1559 (2017).
- [7] S. Sunada, Large Sagnac frequency splitting in a ring resonator operating at an exceptional point, *Phys. Rev. A* **96**, 033842 (2017).
- [8] W. Langbein, No exceptional precision of exceptional-point sensors, *Phys. Rev. A* **98**, 023805 (2018).
- [9] N. A. Mortensen, P. A. D. Gonçalves, M. Khajavikhan, D. N. Christodoulides, C. Tserkezis and C. Wolff, Fluctuations and noise-limited sensing near the exceptional point of parity-time-symmetric resonator systems, *Optica* **5**, 1342-1346 (2018).
- [10] C. Chen, L. Jin and R. B. Liu, Sensitivity of parameter estimation near the exceptional point of a non-Hermitian system, *New J. Phys.* **21**, 083002 (2019).
- [11] M. Z. Zhang, W. Sweeney, C. W. Hsu, L. Yang, A. D. Stone and L. Jiang, Quantum noise theory of exceptional point amplifying sensors, *Phys. Rev. Lett.* **123**, 180501 (2019).
- [12] P. Djorwe, Y. Pennec and B. Djafari-Rouhani, Exceptional point enhances sensitivity of optomechanical mass sensors. *Phys. Rev. Appl.* **12**, 024002 (2019).
- [13] M. A. Miri and A. Alù, Exceptional points in optics and photonics, *Science* **363**, eaar7709 (2014).
- [14] J. Wiersig, Prospects and fundamental limits in exceptional point-based sensing, *Nat. Commun.* **11**, 2454 (2020).
- [15] J. Wiersig, Review of exceptional point-based sensors, *Photonics Res.* **8**, 1457-1467 (2020).
- [16] J. C. Budich and E. J. Bergholtz, Non-Hermitian topological sensors, *Phys. Rev. Lett.* **125**, 180403 (2020).

- [17] J. Wiersig, Robustness of exceptional-point-based sensors against parametric noise: The role of Hamiltonian and Liouvillian degeneracies, *Phys. Rev. A* **101**, 053846 (2020).
- [18] Y. L. Wu, P. J. Zhou, T. Li, W. S. Wan and Y. Zou, High-order exceptional point based optical sensor, *Opt. Express* **29**, 6080-6091 (2021).
- [19] M. Khanbekyan and S. Scheel, Enantiomer-discriminating sensing using optical cavities at exceptional points, *Phys. Rev. A* **105**, 053711 (2022).
- [20] D. Anderson, M. Shah and L. Fan, Clarification of the exceptional-point contribution to photonic sensing, *Phys. Rev. Appl.* **19**, 034059 (2023).
- [21] W. C. Wong and J. S. Li, Exceptional-point sensing with a quantum interferometer, *New J. Phys.* **25**, 033018 (2023).
- [22] Y. Ashida, Z. P. Gong and M. Ueda, Non-Hermitian physics, *Adv. Phys.* **69**, 249-435 (2020).
- [23] X. W. Luo, C. W. Zhang and S. W. Du, Quantum squeezing and sensing with pseudo-anti-parity-time symmetry, *Phys. Rev. Lett.* **128**, 173602 (2022).
- [24] L. Bao, B. Qi, D. Dong and F. Nori, Fundamental limits for reciprocal and nonreciprocal non-Hermitian quantum sensing, *Phys. Rev. A* **103**, 042418 (2021).
- [25] M. V. Berry, Physics of non-Hermitian degeneracies, *Czech. J. Phys.* **54**, 1039-1047 (2004).
- [26] W. D. Heiss, Exceptional points of non-Hermitian operators, *J. Phys. Math. Gen.* **37**, 2455 (2004).
- [27] W. D. Heiss, The physics of exceptional points, *J. Phys. A* **45**, 444016 (2012).
- [28] R. Fleury, D. Sounas and A. Alù, An invisible acoustic sensor based on parity-time symmetry, *Nat. Comm.* **6**, 5905 (2015).
- [29] H. Hodaie, A. U. Hassan, S. Wittek, H. Garcia-Gracia, R. El-Ganainy, D. N. Christodoulides and M. Khajavikhan, Enhanced sensitivity at higher-order exceptional points, *Nature* **548**, 187-191 (2017).
- [30] W. J. Chen, Ş. K. Özdemir, G. M. Zhao, J. Wiersig and L. Yang, Exceptional points enhance sensing in an optical microcavity, *Nature* **548**, 192-196 (2017).
- [31] J. Zhang, B. Peng, Ş. K. Özdemir, K. Pichler, D. O. Krimer, G. M. Zhao, F. Nori, Y. X. Liu, S. Rotter and L. Yang, A phonon laser operating at an exceptional point, *Nat. Photon.* **12**, 479-484 (2018).
- [32] Y. H. Lai, Y. K. Lu, M. G. Suh, Z. Q. Yuan and K. Vahala, Observation of the exceptional-point-enhanced Sagnac effect, *Nature* **576**, 65-69 (2019).
- [33] Z. C. Xiao, H. N. Li, T. Kottos, A. Alù, Enhanced sensing and nondegraded thermal noise performance based on \mathcal{PT} -symmetric electronic circuits with a sixth-order exceptional point, *Phys. Rev. Lett.* **123**, 213901 (2019).
- [34] M. Naghiloo, M. Abbasi, Y. N. Joglekar and K. W. Murch, Quantum state tomography across the exceptional point in a single dissipative qubit, *Nat. Phys.* **15**, 1232-1236 (2019).
- [35] J. H. Park, A. Ndao, W. Cai, L. Hsu, A. Kodigala, T. Lepetit, Y. H. Lo and B. Kanté, Symmetry-breaking-induced plasmonic exceptional points and nanoscale sensing, *Nat. Phys.* **16**, 462-468 (2022).
- [36] R. Kononchuk, J. Z. Cai, F. Ellis, R. Thevamaran and T. Kottos, Exceptional-point-based accelerometers with enhanced signal-to-noise ratio, *Nature* **607**, 697-702 (2022).
- [37] H. Jiang, W. D. Zhang, G. W. Lu, L. L. Ye, H. Lin, J. L. Tang, Z. H. Xue, Z. Li, H. T. Xu and Q. H. Gong, Exceptional points and enhanced nanoscale sensing with a plasmon-exciton hybrid system, *Photonics Res.* **10**, 557-563 (2022).
- [38] Z. P. Li, C. H. Li, Z. Xiong, G. Q. Xu, Y. R. Wang, X. Tian, X. Yang, Z. Liu, Q. H. Zeng, R. Z. Lin, Y. Li, J. K. W. Lee, J. S. Ho and C. W. Qiu, Stochastic exceptional points for noise-assisted sensing, *Phys. Rev. Lett.* **130**, 227201 (2023).
- [39] L. Y. Ding, K. Y. Shi, Q. X. Zhang, D. N. Shen, X. Zhang and W. Zhang, Experimental determination of \mathcal{PT} -symmetric exceptional points in a single trapped ion, *Phys. Rev. Lett.* **126**, 083604 (2021).
- [40] Y. Wu, W. Q. Liu, J. P. Geng, X. R. Song, X. Y. Ye, C. K. Duan, X. Rong and J. F. Du, Observation of parity-time symmetry breaking in a single-spin system, *Science* **364**, 878-880 (2019).
- [41] S. Yu, Y. Meng, J. S. Tang, X. Y. Xu, Y. T. Wang, P. Yin, Z. J. Ke, W. Liu, Z. P. Li, Y. Z. Yang, G. Chen, Y. J. Han, C. F. Li and G. C. Guo, Experimental investigation of quantum \mathcal{PT} -enhanced sensor, *Phys. Rev. Lett.* **125**, 240506 (2020).
- [42] Y. Chu, Y. Liu, H. Liu and J. Cai, Quantum sensing with a single-qubit pseudo-Hermitian system, *Phys. Rev. Lett.* **124**, 020501 (2020).
- [43] See Supplemental Materials for details.
- [44] X. Y. Xu, Y. J. Han, K. Sun, J. S. Xu, J. S. Tang, C. F. Li and G. C. Guo, Quantum simulation of Landau-Zener model dynamics supporting the Kibble-Zurek mechanism, *Phys. Rev. Lett.* **112**, 035701 (2014).
- [45] N. Tischler, C. Rockstuhl and K. Słowik, Quantum optical realization of arbitrary linear transformations allowing for loss and gain, *Phys. Rev. X* **8**, 021017 (2018).
- [46] L. Xiao, K. K. Wang, X. Zhan, Z. H. Bian, K. Kawabata, M. Ueda, W. Yi and P. Xue, Observation of critical phenomena in parity-time-symmetric quantum dynamics, *Phys. Rev. Lett.* **123**, 230401 (2019).
- [47] K. K. Wang, L. Xiao, J. C. Budich, W. Yi and P. Xue, Simulating exceptional non-Hermitian metals with single-photon interferometry, *Phys. Rev. Lett.* **127**, 026404 (2021).
- [48] G. C. Knee and E. M. Gauger, When amplification with weak values fails to suppress technical noise, *Phys. Rev. X* **4**, 011032 (2014).
- [49] F. X. Xu, X. M. Zhang, L. Xu, T. Jiang, M. H. Yung and L. J. Zhang, Experimental quantum target detection approaching the fundamental Helstrom limit, *Phys. Rev. Lett.* **127**, 040504 (2021).

Supplemental Materials for “Non-Hermitian sensing in the absence of exceptional points”

In the supplemental material, we provide general non-Hermitian configurations for enhanced sensing, and the effect of the background noise on the non-Hermitian sensing.

General non-Hermitian configurations for enhanced sensing

In the main text, we demonstrate the pseudo-Hermitian scenario for non-Hermiticity enhanced sensing without involving exceptional points. In this section, we elaborate on more general non-Hermitian sensing configurations in the proposed theoretical framework while going beyond the pseudo-Hermitian scenario based on the population-matching condition, i.e., $|\mathcal{D}_t| \simeq |\delta|$. Recalling that

$$\mathcal{D}_t = \frac{1 + ae^{i2\mathcal{E}t}}{1 - e^{i2\mathcal{E}t}} = \frac{1}{2} [(1 - a) + i(1 + a) \cot \mathcal{E}t], \quad (\text{S1})$$

the population-matching condition, i.e., $|\mathcal{D}_t| \simeq |\delta|$ is achieved by requiring $a = 1$ and $\mathcal{E}t \approx \frac{\pi}{2}$ corresponding to the pseudo-Hermitian scenario in the main text.

Here we point out that the population-matching condition $|\mathcal{D}_t| \simeq |\delta| \ll 1$ may also be satisfied by non-Hermitian systems with complex energy splitting, i.e., $2\mathcal{E} = \omega + i\gamma$. In this case, the eigenstates may not be fully symmetric, for example, $|\phi_+\rangle \sim |0\rangle + \delta|1\rangle$ and $|\phi_-\rangle \sim |0\rangle - (\delta/a)|1\rangle$ with $a \in (0, 1)$. Correspondingly, the Hamiltonian of the bare non-Hermitian sensor can be expressed as the following more general form

$$\mathcal{H} = \frac{\omega + i\gamma}{1 + a} \begin{pmatrix} 1 & \frac{a}{\delta} \\ \delta & a \end{pmatrix}. \quad (\text{S2})$$

The pseudo-Hermitian scenario Hamiltonian in the main text corresponds to $a = 1$ and $\gamma = 0$. We note that, if $a \gtrsim |\delta|$, by choosing a negative value of γ , the condition of $|\mathcal{D}_t| \simeq |\delta|$ can be reached in the neighboring region of $ae^{-\gamma t} = 1$ and $\omega t = \pi$, which leads to that $\mathcal{D}_t = 0$. Moreover, the value of a can even be much smaller than $|\delta|$, e.g. $a = |\delta|^2$, such that the two eigenstates of the non-Hermitian sensor are orthogonal to each other. In this case, we can set $e^{-\gamma t} = |\delta|^{-1}$ to approximately achieve the sensitive non-Hermitian region supported by the condition $|\mathcal{D}_t| \simeq |\delta| \ll 1$. In Fig.S1, we demonstrate the response behavior of three different non-Hermitian sensing configurations for values of a in those different regions. The external perturbing field is assumed to be described by the Hamiltonian $V = \lambda\sigma_x$.

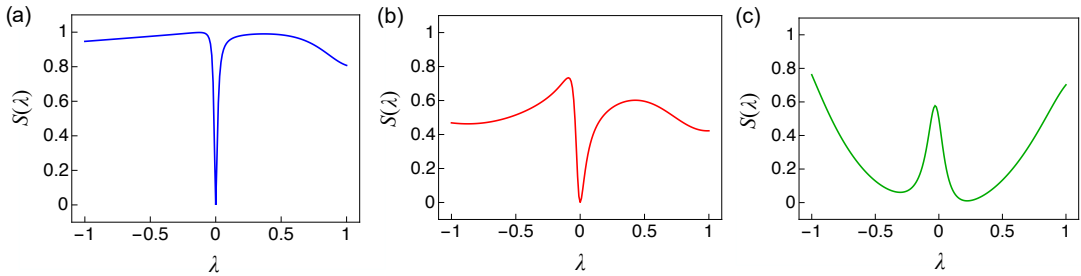


FIG. S1. The normalized population $S(\lambda)$ of the state $|0\rangle$ for different non-Hermitian sensing configurations. From the left to right panels, the values of a are set as $a = e$ for (a), $a = \delta$ for (b) and $a = |\delta|^2$ for (c) respectively. It can be seen that the population signal shows a significant change for a small perturbing field λ . Here we choose the parameter $\delta = 0.05$, $\gamma = -1$, $\{\omega, t\} = \{-\pi/\log a, -\log a\}$ in (a)-(b), and $\{\omega, t\} = \{-\pi/(2\log \delta), -\log \delta\}$ in (c).

As an detailed example, we derive an explicit non-Hermitian Hamiltonian that serves as a sensor and examine its performance. The Hamiltonian is given as

$$\mathcal{H} = \sigma_x + (c + id)\sigma_z, \quad (\text{S3})$$

where $c, d \in \mathbb{R}$ and $\sigma_{x,y,z}$ are Pauli matrices. There are no pertinent symmetries in the Hamiltonian \mathcal{H} . We take into account an external weak field $V = \lambda\sigma_x$, as demonstrated in the main text. Consequently, the coupled Hamiltonian is denoted by

$$H = \mathcal{H} + V = (1 + \lambda)\sigma_x + (c + id)\sigma_z. \quad (\text{S4})$$

For simplicity, we fix the parameters $c = 0.75$, $d = -0.5$, and the evolution time $t = 5.45$. As illustrated in Fig. S2, we experimentally characterize the normalized population of the state $|0\rangle$ and the susceptibility χ_λ . The maximum susceptibility $|\chi_\lambda|_{\max} = 71 \pm 2$ for the non-Hermitian sensor is shown in Fig. S2(b). Its Hermitian counterpart $|\chi_\lambda|_{\max} = 6.3 \pm 0.2$ is shown in Fig. S2(d). In consequence, the non-Hermitian enhancement ratio in $|\chi_\lambda|_{\max}$ is 11.3.

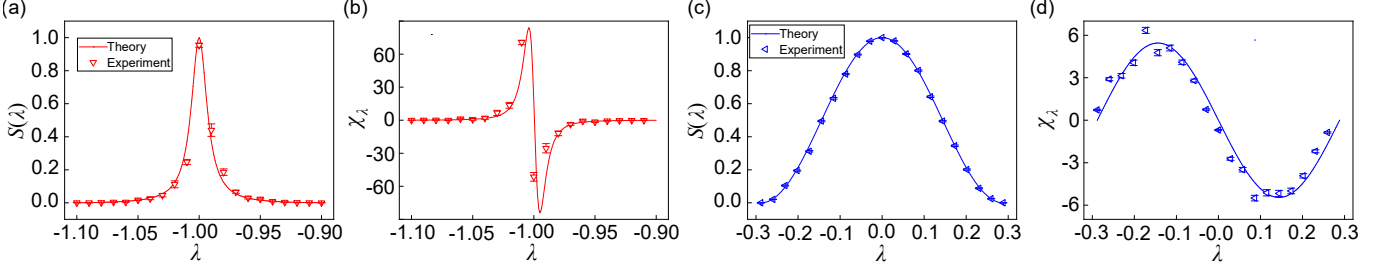


FIG. S2. The normalized population $S(\lambda)$ of the state $|0\rangle$ and the susceptibility χ_λ of the non-Hermitian and Hermitian sensors, respectively. (a)-(b) $S(\lambda)$ and χ_λ for the non-Hermitian sensor. (c)-(d) $S(\lambda)$ and χ_λ for the Hermitian counterpart. The symbols with error bars denote the experimental data, while the curves represent the theoretical prediction obtained by numerical simulations. Error bars are due to the statistical uncertainty in photon-number-counting. The initial state is chosen as $|0\rangle$ and the cycles of evolution are set to $n = 5$.

The effect of the background noise

In this part, we analyze the performance of the non-Hermitian sensor compared to its Hermitian counterpart when considering the background noise. The counts of the horizontally polarized photons N'_H and vertically polarized ones N'_V are registered in the measurement stage and are used to determine the performance of the non-Hermitian sensor with the background noise. Then, the population can be written as follows,

$$\begin{aligned}
 \bar{S}' &= \frac{N_H + N'_H}{N_H + N'_H + N_V + N'_V} = \frac{N_H}{N_H + N_V} \frac{1 + \frac{N'_H}{N_H}}{1 + \frac{N'_H + N'_V}{N_H + N_V}} \\
 &\approx \frac{N_H}{N_H + N_V} \left(1 + \frac{N'_H}{N_H}\right) \left(1 - \frac{N'_H + N'_V}{N_H + N_V}\right) \\
 &\approx \frac{N_H}{N_H + N_V} \left(1 + \frac{N'_H}{N_H} - \frac{N'_H + N'_V}{N_H + N_V}\right) \\
 &= \frac{N_H}{N_H + N_V} \left[1 + \frac{N_V N'_H - N_H N'_V}{N_H(N_H + N_V)}\right] \\
 &= \bar{S} + (1 - \bar{S}) \frac{N'_H}{N} - \bar{S} \frac{N'_V}{N} \\
 &= \bar{S} + \frac{1}{2} (1 - \bar{S}) \eta_H - \frac{1}{2} \bar{S} \eta_V,
 \end{aligned} \tag{S5}$$

where $\eta_{H,V} = N'_{H,V}/N$ is the noise strength, $N = N_H + N_V$ and N_H and N_V are the counts of the horizontally polarized photons and vertically polarized ones in the case without noise, respectively. When $\frac{N'_H + N'_V}{N_H + N_V} \ll 1$ is satisfied, we assume $\frac{1}{1 + \frac{N'_H + N'_V}{N_H + N_V}} \approx 1 - \frac{N'_H + N'_V}{N_H + N_V}$ in the equation above. In general, the background noise is completely random and uniform. We then have the photon counts $N'_H \in [0, \eta_H N]$ and $N'_V \in [0, \eta_V N]$. Hence, the ratios $N'_H/N \in [0, \eta_H]$ and $N'_V/N \in [0, \eta_V]$ are also random and uniform.

The standard deviation of \bar{S}' is developed by the relationship of the error transmission function based on Eq. (S5) as

$$\begin{aligned}
 \Delta \bar{S}'^2 &= \left(\frac{\partial \bar{S}'}{\partial \bar{S}} \Delta \bar{S}\right)^2 + \left(\frac{\partial \bar{S}'}{\partial N'_H/N} \Delta \frac{N'_H}{N}\right)^2 + \left(\frac{\partial \bar{S}'}{\partial N'_V/N} \Delta \frac{N'_V}{N}\right)^2 \\
 &= \left(1 - \frac{\eta_H + \eta_V}{2}\right)^2 \Delta \bar{S}^2 + \frac{1}{12} \left[(1 - \bar{S})^2 \eta_H^2 + \bar{S}^2 \eta_V^2\right],
 \end{aligned} \tag{S6}$$

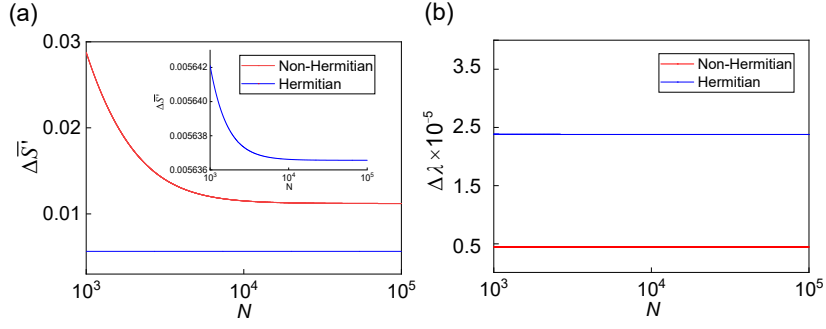


FIG. S3. (a) The standard deviation of \bar{S} as a function of N . (b) The standard deviation of λ . The red curves denote the non-Hermitian sensor, while the blue curves represent the results of its Hermitian counterpart. We choose the parameters $\eta_H = 0.05$ and $\eta_V = 0.06$. We also fix $\bar{S} = 0.34$ for the non-Hermitian sensor and $\bar{S} = 0.5$ for its Hermitian counterpart to get the maximum susceptibility.

where $\Delta\bar{S}^2 = \frac{N_H N_V}{p N^3}$ is the standard deviation for the non-Hermitian sensor and p is the success probability, while $\Delta\bar{S}^2 = \frac{N_H N_V}{N^3}$ is for its Hermitian counterpart. In Eq. (S6), the first term which is from the fluctuation of single photons, tends to 0 when $N \gg 1$, even if the success probability is considered. Whereas, the second term results in a constant that is independent of N . Based on the above analysis, we can approximate the minimum measurement uncertainty through $\Delta\lambda \simeq \Delta\bar{S}'/|\chi|_{\max}$. Therefore, the ratio of the minimum measurement uncertainty between non-Hermitian and Hermitian sensors is $\Delta\lambda_{\text{non-H}}/\Delta\lambda_{\text{H}} = |\chi|_{\max}^{\text{H}}/|\chi|_{\max}^{\text{non-H}}$. The corresponding results are presented in Fig. S3, which agree with the above derivation.

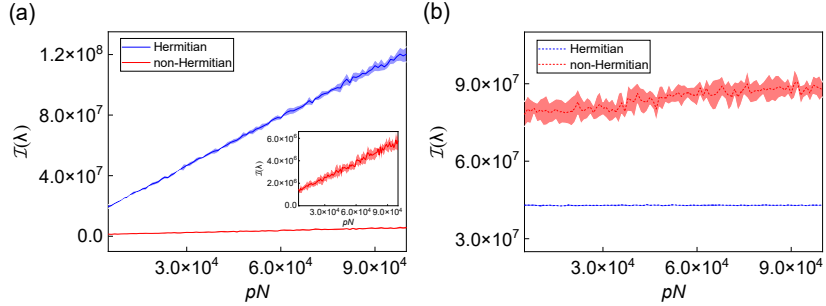


FIG. S4. The Fisher information as a function of N without and with the background noise in (a) and (b), respectively. The strength of noise is fixed at $\eta_H = \eta_V = 0.1$. The shaded area indicates the standard deviation.

To further illustrate the background noise's effect, we numerically calculate the Fisher information for both non-Hermitian and Hermitian sensors in the presence of the background noise. The Fisher information is defined by [1]

$$\mathcal{I}(\lambda) = \int f_N(\bar{S}'|\lambda) \left(\frac{\partial}{\partial \lambda} \log f_N(\bar{S}'|\lambda) \right)^2 d\bar{S}', \quad (\text{S7})$$

where $f_N(\bar{S}'|\lambda)$ is the probability density function for the random variable \bar{S}' defined in Eq. (S6), conditioned on the value of λ . In Fig. S4, we show the Fisher information as a function of N . Importantly, the Fisher information for both the Hermitian and non-Hermitian scenarios in presence of the background measurement noise, instead of satisfying $\mathcal{I}(\lambda) \propto N$, would reach a plateau for a sufficiently large $N \gg 1$. This behavior is consistent with the feature of technical experiment noises that cannot be averaged out by repetitive measurements [2]. However, the non-Hermitian scenario can help us to achieve a larger Fisher information with respect to the parameter λ , which is attributed to the non-Hermitian-enhanced susceptibility, i.e., $|\chi|_{\max}^{\text{non-H}} \gg |\chi|_{\max}^{\text{H}}$. The results reveal that the non-Hermitian sensor indeed improves the performance of the parameter estimation.

* These authors contributed equally to this work.

† wyz@ustc.edu.cn

‡ jianmingcai@hust.edu.cn

§ gnep.eux@gmail.com

- [1] R. A. Fisher, Theory of statistical estimation, *Math. Proc. Camb. Phil. Soc.* **22**, 700 (1925).
 - [2] A. N. Jordan, J. Martínez-Rincón and J. C. Howell, Technical advantages for weak-value amplification: When less is more, *Phys. Rev. X* **4**, 011031 (2014).
-